Stem Cells Translational Medicine, 2022, **11**, 1040–1051
https://doi.org/10.1093/stcltm/szac061
Advance access publication 26 August 2022
Original Research

Metabolic Maturation Increases Susceptibility to Hypoxia-induced Damage in Human iPSC-derived Cardiomyocytes

Marijn C. Peters[1], Renee G.C. Maas[1], Iris van Adrichem[1], Pieter A.M. Doevendans[1], Mark Mercola[2], Tomo Šarić[3], Jan W. Buikema[1], Alain van Mil[1], Steven A.J. Chamuleau[1,4], Joost P.G. Sluijter[1], Anna P. Hnatiuk[2,‡], Klaus Neef[1,‡,*]

[1]Department of Cardiology, Laboratory of Experimental Cardiology, Regenerative Medicine Centre Utrecht, University Medical Centre Utrecht, University Utrecht, Utrecht, The Netherlands
[2]Cardiovascular Institute and Department of Medicine, Stanford University, Stanford, CA, USA
[3]Center for Physiology and Pathophysiology, Institute for Neurophysiology, Faculty of Medicine and University Hospital Cologne, University of Cologne, Cologne, Germany
[4]Department of Cardiology, Amsterdam UMC Heart Center, Amsterdam, The Netherlands

*Corresponding author: Klaus Neef, PhD, Department of Cardiology, Laboratory of Experimental Cardiology, Regenerative Medicine Utrecht, University Medical Centre Utrecht, Heidelberglaan 100, 3584CX Utrecht, The Netherlands. Email: k.neef@umcutrecht.nl
‡Contributed equally.

Abstract

The development of new cardioprotective approaches using in vivo models of ischemic heart disease remains challenging as differences in cardiac physiology, phenotype, and disease progression between humans and animals influence model validity and prognostic value. Furthermore, economical and ethical considerations have to be taken into account, especially when using large animal models with relevance for conducting preclinical studies. The development of human-induced pluripotent stem cell-derived cardiomyocytes (iPSC-CMs) has opened new opportunities for in vitro studies on cardioprotective compounds. However, the immature cellular phenotype of iPSC-CMs remains a roadblock for disease modeling. Here, we show that metabolic maturation renders the susceptibility of iPSC-CMs to hypoxia further toward a clinically representative phenotype. iPSC-CMs cultured in a conventional medium did not show significant cell death after exposure to hypoxia. In contrast, metabolically matured (MM) iPSC-CMs showed inhibited mitochondrial respiration after exposure to hypoxia and increased cell death upon increased durations of hypoxia. Furthermore, we confirmed the applicability of MM iPSC-CMs for in vitro studies of hypoxic damage by validating the known cardioprotective effect of necroptosis inhibitor necrostatin-1. Our results provide important steps to improving and developing valid and predictive human in vitro models of ischemic heart disease.

Key words: hypoxia; cardiomyocytes; metabolic maturation; induced pluripotent stem cells (iPSC); ischemia; damage.

Graphical Abstract

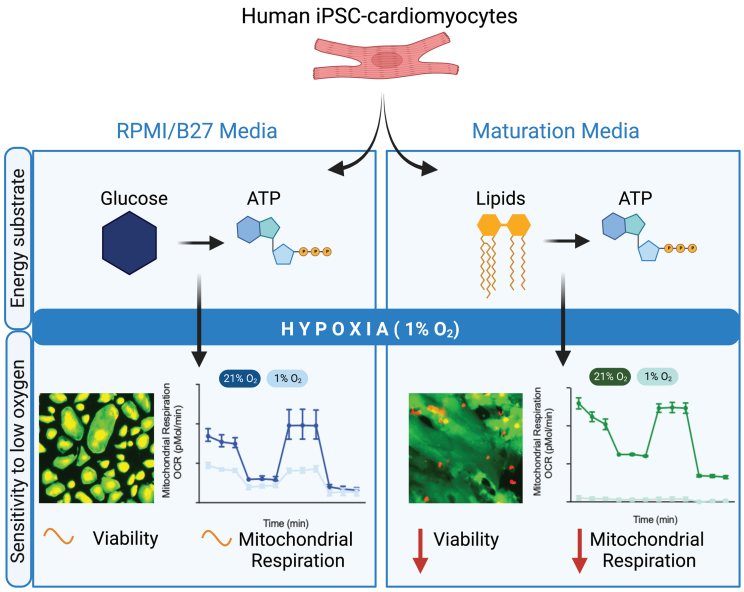

Received: 23 April 2022; Accepted: 12 July 2022.

Significance Statement

The immaturity of human iPSC-derived cardiomyocytes (iPSC-CMs) remains a roadblock for disease modeling. This study shows that only after metabolic maturation in low glucose, high oxidative substrate media, iPSC-CMs become susceptible to hypoxia-induced cellular damage. Inhibition of necroptosis prevented the hypoxia-induced decrease in mitochondrial respiration and cell death in metabolically matured iPSC-CMs. Together, these findings suggest that metabolically matured iPSC-CMs are susceptible to hypoxia damage, representing a key step for establishing valid in vitro models of cardiac ischemia.

Introduction

Ischemic heart disease is a major cause of death worldwide.[1] The decrease in oxygen and nutrient availability in the myocardium leads to cardiomyocyte (CM) death and therefore loss of cardiac contractile force.[2] Current clinical therapies focus on early reperfusion of the ischemic tissue, thereby decreasing the tissue damage which occurs after myocardial infarctions. To develop improved therapeutic approaches to protect the heart from ischemic damage, both animal models and in vitro disease modeling platforms have been used frequently. However, although cardioprotective factors have shown promising therapeutic effects in in vitro cell models and in animal experiments, they often failed in showing clear beneficial effects in clinical trials.[3] The roles of comorbidities, aging, and the use of medication, often neglected in preclinical models, have been considered as reasons for translational failure.[4] Moreover, existing models do not robustly reflect the human CM-specific pathophysiology due to marked differences between CMs from humans compared to other species,[5] for example, with respect to calcium handling,[6] electrophysiology,[6] myofilament composition,[7,8] maturation expression profile,[9] and metabolism.[10] The development of human-induced pluripotent stem cell (iPSC) technology[11] and their differentiation to CMs[12] opened doors for more suitable human-based cardiac disease modeling by the generation of patient-specific CMs[13] and preclinical screening of therapeutics.[14,15] Despite the mentioned advantages linked to their human origin, iPSC-CMs, typically derived from a 20-day differentiation protocol, display a fetal rather than adult CM phenotype.[16,17] Adult human CMs generate 90% of their energy from mitochondrial oxidative phosphorylation while neonatal rat CMs and iPSC-CMs use glycolysis as their main energy source,[18] as reflected in a lower expression of TCA cycle and fatty acid β-oxidation markers.[19,20] Thus, human iPSC-CMs can have limited clinical validity and predictive value as models of pathophysiological processes, especially when linked to oxidative metabolic processes.[19,21] Several studies focused on increasing the maturation of iPSC-CMs by stimulating the postnatal shift from anaerobic glycolysis-dependent metabolism to aerobic β-oxidation.[18,22-24] Recently, a study showed increased cell death of metabolically matured (MM) iPSC-CMs for 8 days in glucose-deprived, fatty acid-rich media, upon submission to in vitro ischemia-reperfusion injury by applying 2 hours of complete oxygen deprivation (0% O_2) followed by 4 hours of reperfusion (20% O_2).[25] In a similar attempt, we have shown that 3 weeks of culture in a medium with physiological levels of glucose and Ca^{2+} supplemented with a fine-tuned composition of additives, induced metabolic, structural, electrophysiological, and mechanical iPSC-CM maturation characterized by lower resting membrane potential, rapid depolarization, increased sarcoplasmic reticulum calcium cycling, increased contractile force and enhanced fatty acid oxidation, in line with CM maturation during cardiac development.[18]

In this study, we sought to investigate the utilization of MM iPSC-CMs to model cardiac ischemic damage and exemplarily evaluate the cardioprotective effect of the RIP1 kinase inhibitor necrostatin-1.

Materials and Methods

Cell Culture

The female iPSC line SCVI-273 (Sendai virus reprogrammed) was kindly provided by Joseph Wu, Stanford University.[26] The female iPSC line NP0141-31B was generated in the Šarić group from peripheral blood mononuclear cells, also using the Sendai virus reprogramming method.[27,28] This line is deposited as cell line UKKi032-C at the European Bank for induced Pluripotent Stem Cells (EBiSC, www.ebisc.org) and is listed at the international online registry hPSCreg (www.hpscreg.eu). iPSCs were cultured in Essential 8 medium (Gibco, A1517001) in 0.1 mg/mL matrigel-coated 6-well plates (Corning, CLS356252). When reaching 80%-90% confluence, directed differentiation to CMs was initiated by changing medium to RPMI 1640 (Thermo Fisher Scientific, 11875085) supplemented with 2% B27 minus insulin (Thermo Fisher Scientific, A1895601) (B27-medium) and 7 µM CHIR99021 (Selleck Chemicals, S2924). After 3 days, B27-medium was changed and supplemented with 2 µM Wnt-C59 (R&D Systems, 5148) to inhibit canonical Wnt signaling. On day 7, the medium was changed to RPMI 1640 and 2% B27 plus insulin supplement (Thermo Fisher Scientific, 17504001) (B27+ medium) and on day 9 to RPMI 1640 without glucose (Thermo Fisher Scientific, 118979020) and 2% B27 plus insulin for purification (depletion of non-CM cells). On day 11, cells were re-plated in RPMI/B27 plus insulin supplemented with 10% KnockOut Serum Replacement (KOSR, Thermo Fisher Scientific, 108280028) and 10 µM selective Rock-1 inhibitor Y-27632 (Selleck Chemicals, S1049). After the second purification on day 14 for 2 days in RPMI 1640 without glucose, the medium was changed to RPMI/B27 plus insulin. On day 20, the purification medium was changed to maturation medium,[18] or cells were kept in RPMI/B27 plus insulin. Cells were matured in maturation medium for 3 weeks before re-plating with medium changes every 4 days.

Damage Induction

Four days before applying hypoxic conditions at day 20, the medium was changed to medium containing variable nutrient compositions (Supplementary Table 1). Ischemia was induced by incubation at 5% O_2 in a hypoxia incubator (In-VitroCell NU-5800, NuAire) providing continuous oxygen monitoring or ~1% O_2 using the GasPak EZ Pouch system (BD, 260683) with indicator strips to confirm O_2 concentrations below 1%.

Preconditioning Protective Treatment

Before hypoxia, the medium was changed to media of variant nutrient composition (Supplementary Table 1). iPSC-CMs were preconditioned with 60 µM necroptosis inhibitor necrostatin-1 (Nec-1, Abcam ab141053) for 24 hours.

Lactate Dehydrogenase, Glucose, and Lactate Measurements

Media glucose and lactate levels were determined using the Accutrend plus device (Roche, 05050472023) and verified using the glucose (Sigma, MAK083-1KT) and lactate colorimetric kits (Sigma, MAK064-1KT). Lactate dehydrogenase levels were determined using the LDH assay colorimetric kit (Abcam, ab102526) according to the manufacturer's instructions.

Immunofluorescent Staining

Live dead assay was performed using EthD1/calcein AM staining with the LIVE/DEAD Kit, for mammalian cells (Thermo Fisher Scientific, L3224) according to the manufacturer's instructions, and imaging was performed using the EVOS Floid microscope (Thermo Fisher Scientific, AMF5000). The ratio of EthD1 to calcein AM was determined by dividing the number of EthD1-positive cells by the number of calcein AM-positive cells per image. The averages of 5 images were used per condition. For immunofluorescence stainings, after fixation in 4% paraformaldehyde for 30 minutes, cells were permeabilized in 0.1% Triton X-100 (Sigma, 11332481001) before blocking in 10% normal goat serum/1% BSA (Sigma, A9418). Primary antibodies used were: ACTN1 (Sigma-Aldrich, A7811, 1:200), cardiac troponin T (Abcam, ab45932, 1:100), Ki-67 (Abcam, ab8330, 1:200), pH3 (Cell Signaling Technology, #9701, 1:200), TOMM20 (Abcam, ab56783, 1:200) and Aurora B kinase (Abcam, ab2254, 1:100). Detection was mediated by incubation with Alexa Fluor antibody conjugates (Thermo Fisher Scientific) and nuclei were visualized using DAPI (Thermo Fisher Scientific, 62248). Mounting was performed using Fluoromount-G mounting medium (Thermo Fisher Scientific, 00-4958-02). For apoptotic cell death analysis, TUNEL assays (Roche, 11684795910) were performed according to the manufacturer's instructions. Imaging was performed on a confocal microscope (Leica Sp8x, LAS X imaging software) and image analysis using ImageJ (1.51a, Java 1.8.0.231).

Flow Cytometry

Cells were gently dissociated (multi-tissue dissociation kit, Miltenyi Biotec, 130-110-204) and incubated with LIVE/DEAD fixable green dead cell stain kit (Thermo Fisher Scientific, L23101). This kit contains a fixable fluorescent dye that binds to amines. In viable cells, this amine-reactive dye binds amines on the outer cell surface, as opposed to dead cells in which the dye can additionally bind internal amines due to membrane disruption. After staining, cells were fixed (inside fix solution, Miltenyi Biotec, 130-090-477) and stained with primary antibodies (diluted in inside perm solution, Miltenyi Biotec, 130-090-477). ACTN1-VioBlue (Miltenyi Biotec, 130-127-354, 1:10) and cardiac troponin T VioBlue (Miltenyi Biotec, 130-120-402, 1:10) were used as conjugated antibodies. As a control, universal isotype control antibodies (REA, Miltenyi Biotec, 130-096-932) were used. Media and washes were collected to obtain a complete representation, including detached cells. The samples were analyzed using a FACS Canto system (BD Biosciences, FACSDiva software 6.0) and FlowJo software (BD Biosciences, v10).

Beating Rate Analysis

iPSC-CM beating rate was microscopically determined (Olympus CKX53) and recorded (Hero 8 GoPro camera). Beats per minute were quantified by counting the number of contractions of individual cells from 10-second videos.

Seahorse Analysis

Mitochondrial respiration was measured using a XF24 Extracellular Flux Analyzer (Seahorse Bioscience, Agilent) to assess the effect of hypoxia on the electron transport chain complexes. XF24 plates (Agilent, 103518-100) were used and coated with 0.1 mg/mL Matrigel (Corning, CLS356252) before cells were seeded at a density of 1.0×10^5 cells per well. 24 hours or 4 hours before Seahorse analysis, plates were placed in a GasPak EZ Pouch system to induce hypoxia according to the manufacturer's instructions. One hour before measurement, cells were washed three times with Seahorse XF DMEM Basal Medium (Agilent, 103680-100), supplemented with 2% B27, 4 mM glutamine (Gibco, 25030081), 10 mM glucose (Thermo Fisher Scientific, 15023021), and 1% chemically defined lipid concentrate (Thermo Fisher Scientific, 11905031). Oxygen consumption rate (OCR) was determined using XF Cell Mito Stress Assay (Agilent, 103015-100) with subsequent additions of: (1) ATP synthase inhibitor: 2.5 mM oligomycin, (2) uncoupler: 2.5 mM carbonyl cyanide 4-(trifluoromethoxy) phenylhydrazone (FCCP) and (3) complex I/II inhibitors: 2.5 mM rotenone/antimycin A. At the end of the measurement, the OCR values were normalized to cell numbers per well as assessed by Hoechst 33342 (Thermo Fisher Scientific) staining at ×20 magnification imaging using the Evos microscope and ImageJ.[29] Baseline respiration was calculated by subtracting the OCR, after the addition of rotenone and antimycin A, from the respiration as measured at the first time point. ATP production was calculated as the OCR at the first time point minus the OCR after oligomycin infusion. The proton leak was determined by subtracting the OCR after FCCP infusion from the value after oligomycin infusion. Maximal OCR was calculated as the difference between the OCR after FCCP infusion and after rotenone and antimycin A infusion. Respiratory capacity was calculated by subtracting the difference between the OCR before the addition of inhibitors and after rotenone and antimycin A infusion from the OCR after FCCP infusion. Lastly, non-mitochondrial respiration was defined as the OCR after rotenone and antimycin A infusion. The experiment was done in 1-2 biological replicates, with each replicate consisting of 5 technical repeats per condition.

Statistical Analysis

iPSC lines from two donors were used and the number (N) depicted in individual figures represents the number of independent experiments performed. Each experiment was performed with both cell lines. Statistical analysis was performed using Prism 8 (GraphPad) software. Normality was assessed using a Shapiro-Wilk test. To compare two normally distributed groups, a Student's *t*-test was performed. For three or more groups and the assessment of one parameter, one-way ANOVA statistical test was used. With multiple parameters and three or more groups, a two-way ANOVA was

used. For one-way ANOVA and two-way ANOVA, Dunnett's multiple comparison test was used as post hoc analysis to determine significance at $P < .05$. Results are shown as mean ± SEM.

Results

Immature iPSC-CMs Are Not Sensitive to Hypoxia

Human iPSCs were subjected to directed differentiation to cardiomyocytes (iPSC-CMs) using the Wnt pathway inhibition differentiation protocol,[27,28] resulting in a homogeneous, autonomously contractile cell population robustly expressing CM-defining markers troponin T and ACTN1 (Fig. 1A-1C) and only low ratios of cells expressing proliferation marker Ki-67 (5.9% ± 0.8%; Fig. 1D), similar to values reported for neonatal mice and young infant hearts.[30,31]

To test the sensitivity of these, presumably immature, iPSC-CMs to oxygen and nutrient deprivation, we cultured the cells in four different media of variable nutrient compositions (Supplementary Table 1) before exposure to hypoxia: (1) DMEM-Glu/L (25 mM glucose, 10% KOSR), (2) RPMI-Glu/B27 (11.1 mM glucose, 2% B27), (3) RPMI/B27 (0mM glucose, 2% B27), and (4) RPMI-Lac/L (0 mM glucose, lactate, 10% KOSR). DMEM-Glu/L is highest in glucose and lipids, followed by RPMI-Glu/B27 with high glucose and low lipids, where both types are commonly used to maintain iPSC-CMs after differentiation. RPMI/B27 and RPMI-Lac/L are both used during the purification steps of iPSC differentiation into CMs and contain no glucose where RPMI/B27 is low in lipids. RPMI-Lac/L contains additional lactate and higher lipid concentration to inhibit glycolysis and stimulate the use of the respiratory chain.[32]

Incubation in 1% O_2 for 24 hours did not lead to increased cell death of iPSC-CMs in high-glucose media (DMEM-Glu/L, RPMI-Glu/B27) and no-glucose and low-lipid media (RPMI/B27) compared to incubation in 21% O_2 (Fig. 1E, 1F). Only exposure to 1% O_2 for 24 hours in no-glucose, high-lipid and high-lactate medium (RPMI-Lac/L) induced minimal, yet significantly increased cell death (ethidium homodimer-1 [EthD1]/calcein AM ratio: 0.02 ± 0.005 [21% O_2] vs 0.11 ± 0.004 [1% O_2]; $P = .04$). To validate the assessment of cell death, we included a Triton X-100 treatment as a positive control that resulted in 100% cell death for all media conditions (Fig. 1E). To more accurately quantify results, we repeated the respective experiments using RPMI-Lac/L medium and analyzed via flow cytometry using an amine-reactive dye to detect membrane disruption. Although in 12 of 30 experiments a small reduction in cell viability was observed, differences were statistically non-significant in flow cytometric analyses (viable cells: 85% ± 1.9% [21% O_2] vs 78.3 ± 3.0 [1% O_2]; $P = .1$; Fig. 1G, 1H). These findings show immature iPSC-CMs are insensitive to hypoxic damage irrespective of media glucose content. The presence of lipids and lactate in combination with low glucose media led to minimal, yet detectable hypoxic damage in immature iPSC-CMs.

Metabolically Matured iPSC-CMs Are Sensitive to Hypoxia

To investigate whether maturation of iPSC-CMs would increase susceptibility to hypoxia, we applied the recently published protocol for metabolic maturation (MM)[18] (Fig. 2A), resulting in increased ratio of ACTN-expressing cells (83.3% ± 1.3% [RPMI/Lac/L (non-MM)] vs 94.4% ± 2.6% [MM]; $P < .01$; Fig. 2B, 2C) and decreased ratio of proliferating Ki-67-expressing cells (5.9% ± 0.77% [non-MM] vs 1.4% ± 0.32% [MM]; $P < .01$; Fig. 2D). MM iPSC-CMs displayed a significant increase in cell death after 16 and 24 hours of hypoxia (fold increase EthD1/calcein AM ratio compared to normoxic: 1.78 ± 0.14 [1% O_2, 16 hours]; 1.83 ± 0.15 [1% O_2, 24 hours]; Fig. 2E, 2F). Hypoxia-induced damage of MM iPSC-CMs was confirmed by an increase in media lactate dehydrogenase concentration (Fig. 2G) (25.0 ± 0.01 [U/l; 21% O_2] vs 39.4 ± 5.8 [U/l; 1% O_2, 24 hours], $P < .05$) and a reduction in cell viability assessed via flow cytometry (56.5% ± 2.8% [21% O_2] vs 14.0% ± 1.2% [1% O_2, 24 hours]; $P < .001$; Fig. 2H, 2I). Additionally, analyses of iPSC-CM beating rates after 24-hour exposure to 1% O_2 showed significant decrease only for MM (Supplementary Fig. 1).

Although iPSC-CMs are continuously exposed to an atmospheric concentration of 21% O_2 during cell culture conditions, in myocardial tissue, normoxic oxygen concentrations can be substantially lower.[33] We therefore assessed whether a decrease from 21% O_2 to a more physiological cardiac normoxia of 5% O_2 would already induce damage in MM iPSC-CMs (Fig. 3A). Although hypoxia did not change the fraction of ACTN1-positive MM iPSC-CMs in the surviving population (ACTN1$^+$: 92.7 ± 3.35% [24 hours, 21% O2] vs 93.8 ± 1.7%, $P = .74$ [24 hours, 1% O_2]; Supplementary Fig. 2), both, incubation in 5% O_2 and 1% O_2, decreased myofibrillar organization, as shown by immunostaining for ACTN1 and cardiac troponin T (cTnT) (Fig. 3B, 3C).

An increased ratio of apoptotic (TUNEL$^+$) iPSC-CMs was observed in MM after short periods (4 hours) of exposure to 5% O_2 (25.5% ± 1.2%), similar to 1% O_2 (23.7% ± 1.6%), compared to atmospheric 21% O_2 (15.4% ± 0.83%; $P < .05$; Fig. 3D, 3E). Longer hypoxia periods (24 hours) increased percentage of apoptotic iPSC-CMs to 41.5% ± 4.5% (5% O_2) and 37.6% ± 3.5% (1% O_2) compared to 12.0% ± 1.5% (21% O_2; $P < .001$; Fig. 3D, 3E). We did not observe a significant difference in the ratio of apoptotic iPSC-CMs between 5% and 1% O_2, both after short- (4 hours) or long-term (24 hours) incubation. We collected media after hypoxia for 4 and 24 hours to assess glucose, lactate, and lactate dehydrogenase concentrations and found significantly increased glucose consumption after 24 hours at both 5% and 1% O_2, reducing glucose levels below the detection limit of 0.6 mM (Fig. 3F).

Metabolic Profiling of Non-MM and MM iPSC-CMs after Hypoxia Exposure

To investigate whether hypoxia affects the mitochondrial function of iPSC-CMs, we compared the OCRs of MM iPSC-CMs and non-MM iPSC-CMs 40 days after differentiation in normoxia and hypoxia (1% O_2) using Seahorse metabolic analysis. To study the role of glucose in hypoxia-mediated mitochondrial damage in the non-MM iPSCs, we used RPMI-Glu/B27 as high glucose medium and RPMI-Lac/L as low glucose medium (Fig. 1). In normoxia, MM iPSC-CMs showed the highest OCR, indicating increased use of oxidative phosphorylation (Fig. 4A-4C). Under hypoxic conditions, non-MM iPSC-CMs cultured in RPMI-Glu/L maintained responsiveness, while non-MM iPSC-CMs cultured in RPMI-Lac/L lost responsiveness to the mitochondrial respiratory chain inhibitors (Fig. 4A, 4B). Glucose-deprived (RPMI-Lac/L) non-MM iPSC-CMs showed decreased OCR in normoxia compared to non-MM iPSC-CMs in glucose-rich medium (RPMI-Glu/B27) illustrating metabolic starvation

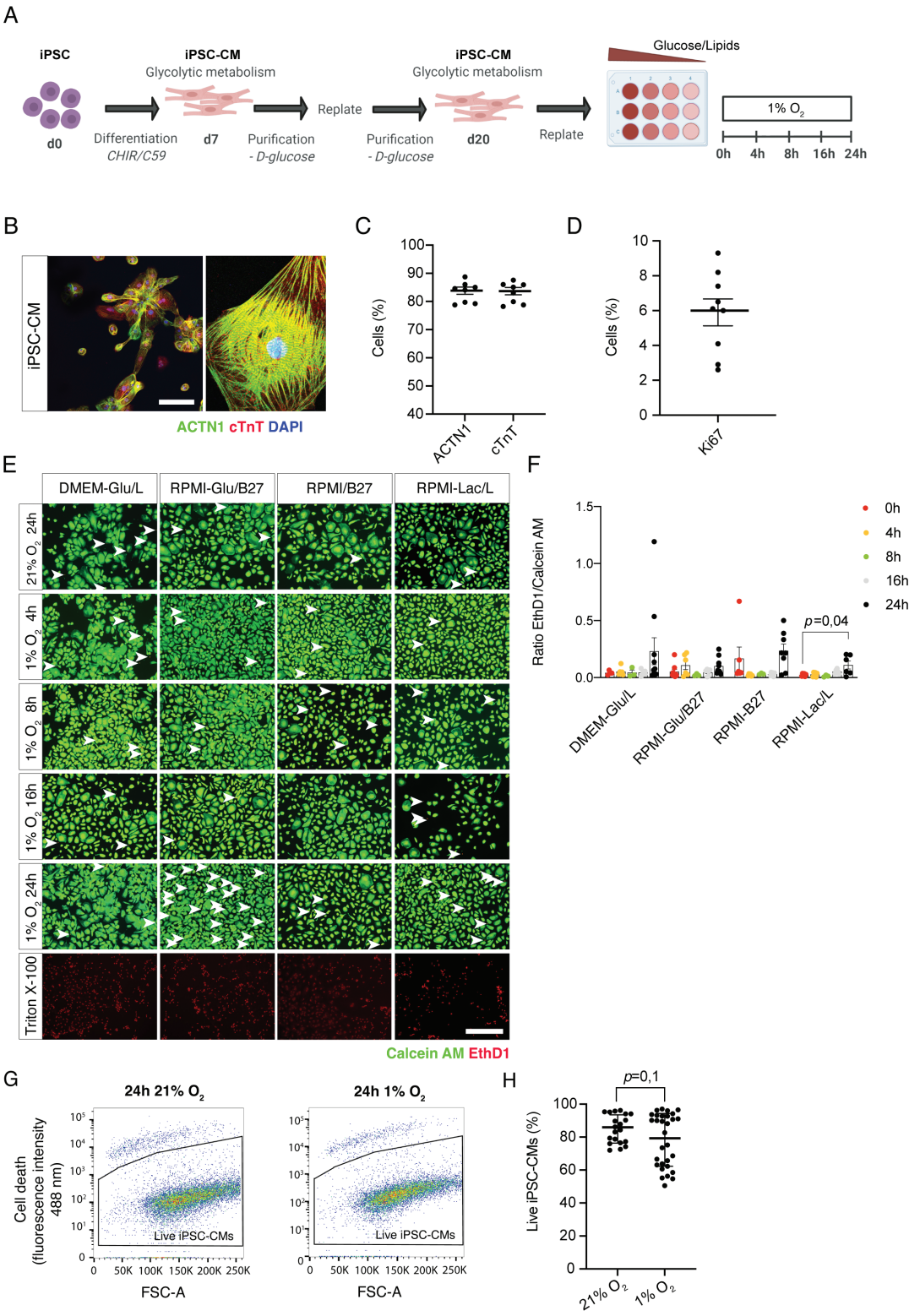

Figure 1. Hypoxia does not induce damage in iPSC-CMs. (A) Schematic representation of experimental setup. (B, C) ACTN1 and cTnT expression of iPSC-CMs assessed by immunofluorescence microscopy (B) and flow cytometry (C) (n = 8). (D) Ki-67 expression of iPSC-CMs assessed by flow cytometry (n = 9). (E) Ethidium homodimer-1 (EthD1)/calcein AM staining of iPSC-CMs cultured in four different media (DMEM-Glu/L, RPMI-Glu/B27, RPMI-B27, RPMI-Lac/L) with indicated nutrient compositions, exposed to indicated O_2 concentrations and durations. Arrowheads indicate a representative selection of EthD1-positive cells. (F) Quantification (n = 8) and media compositions of E. (G) Flow cytometry analysis of the viability of iPSC-CMs cultured for 24 hours in 21% O_2 or 1% O_2 and quantification. (H) (n = 30). Data are collected from 2 to 3 technical replicates (exact amounts specified in separate panels) and 3 biological replicates (cardiac differentiations) of 2 cell lines. H: 3 technical replicates from 10 biological replicates (cardiac differentiations). Data were analyzed using one-way ANOVA and Dunnett's multiple comparison test. *P < .05. Scale bar = 200 µm. Data are shown as mean ± SEM.

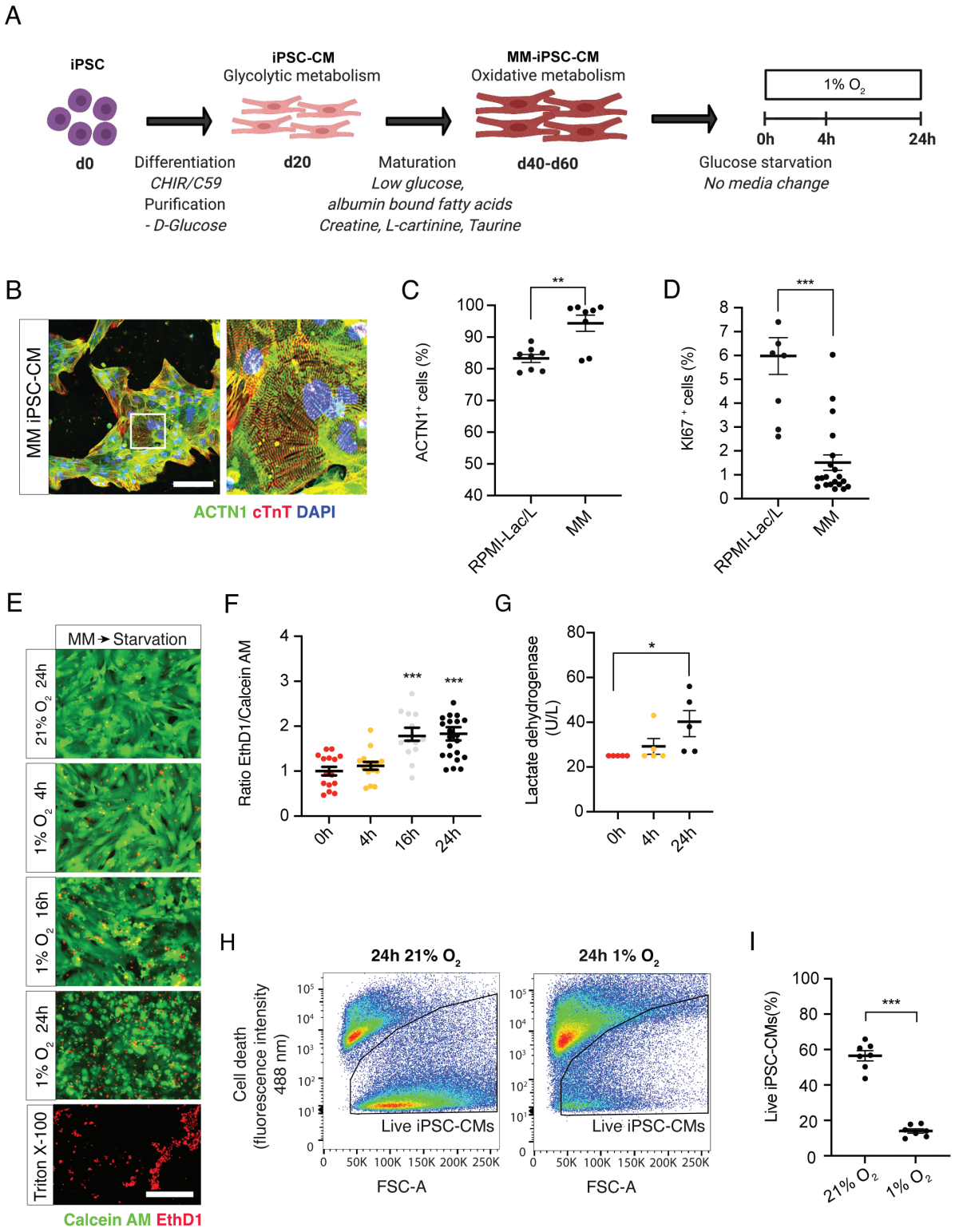

Figure 2. Hypoxia induces cell death of MM iPSC-CMs. (A) Schematic representation of experimental setup. (B, C) ACTN1 and cTnT expression of MM iPSC-CMs by immunofluorescence microscopy (B) and flow cytometric analysis of ACTN1 expression (C) (n = 8, 2 cell lines, 2 biological replicates, 2 technical replicates). (D) Ki-67 expression of MM iPSC-CMs compared to non-MM iPSC-CMs (n = 20, 2 cell lines, 5 biological replicates, 2 technical replicates). (E, F) EthD1/calcein AM staining (LIVE/DEAD assay) of MM iPSC-CMs exposed to 21% O_2 for 24 hours or 1% O_2 for 4, 8, 16, or 24 hours and quantification (F) (n = 15, 2 cell lines, 4 biological replicates, 1-2 technical replicates). (G) Lactate dehydrogenase media levels of day 40 matured iPSC-CMs exposed to 1% O_2 (n = 5, 2 cell lines, 2 biological replicates, 1-2 technical replicates). (H, I) Flow cytometry analysis of MM iPSC-CMs viability after 24-hour exposure to 21% O_2 or 1% O_2 and quantification (I) (n = 7, 2 cell lines, 3 biological replicates, 1-2 technical replicates). Data were analyzed using one-way ANOVA and Dunnett's multiple comparison test. $^{**}P < .01$; $^{***}P < .001$. Scale bar = 200 μm. Data are shown as mean ± SEM.

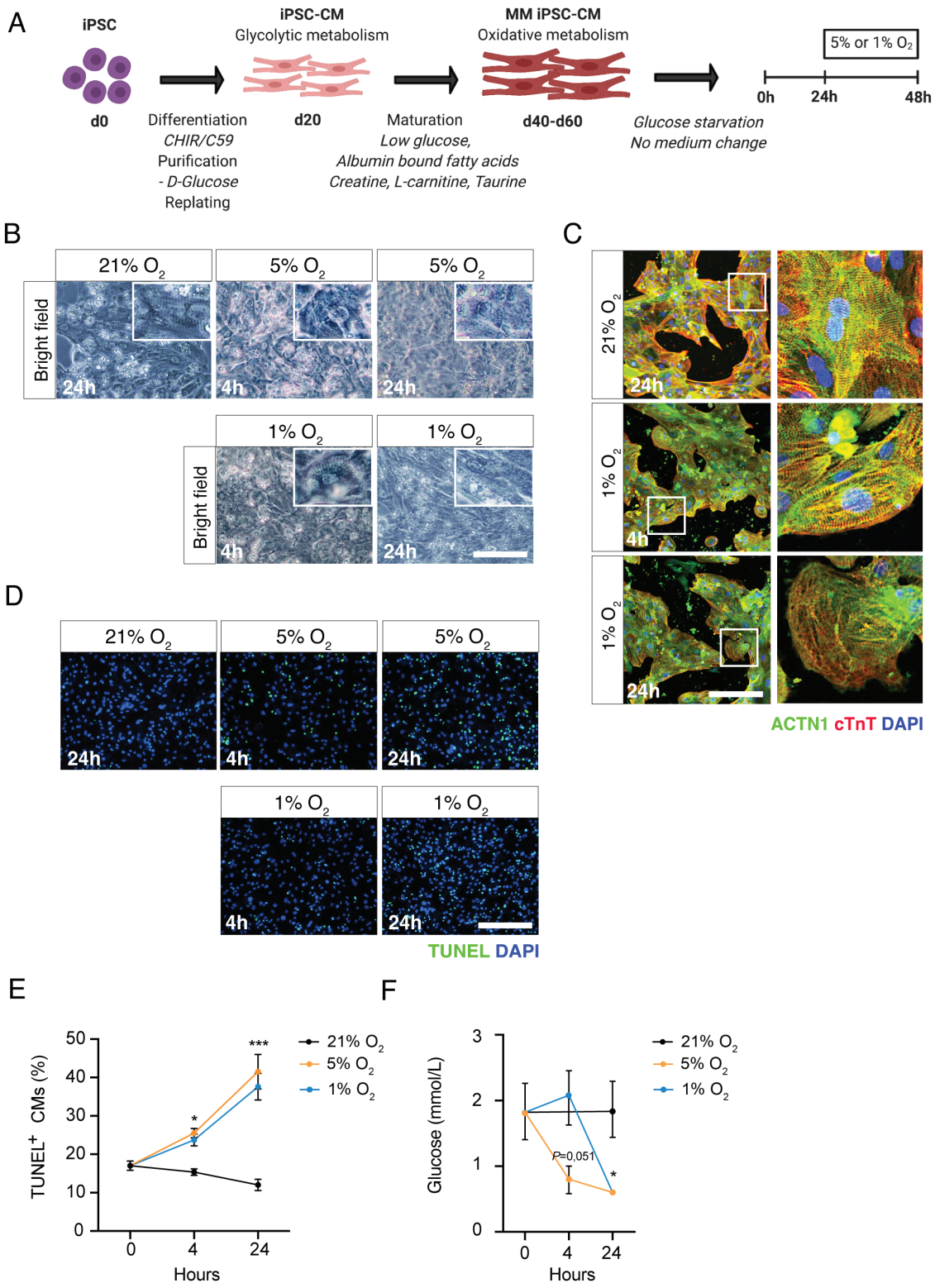

Figure 3. Mild hypoxia is sufficient to induce cell death in MM iPSC-CMs. (A) Schematic representation of experimental setup. (B) Bright-field images of MM iPSC-CMs exposed to indicated hypoxia conditions. (C) Microscopic images of ACTN1 and cTnT immunostainings. Square indicates the area of close-up. (D) Microscopic images of TUNEL staining of MM iPSC-CMs. (E) Quantification of TUNEL staining. (F) Glucose concentration in media after 4- to 24-hour incubation of MM iPSC-CMs at indicated hypoxia conditions. E: 3 technical replicates from 6 biological replicates (cardiac differentiations) (n = 28); F: 2 technical replicates from 3 biological replicates (cardiac differentiations) (n = 5). Data were analyzed using one-way ANOVA and Dunnett's multiple comparison test. *P < .05; ***P < .001. Scale bar = 200 µm. Data are shown as mean ± SEM.

caused by the absence of glucose (Fig. 4A, 4B). While MM iPSC-CMs showed the highest OCR in normoxic conditions and similar responses to the mitochondrial inhibitors as the non-MM iPSC-CMs in glucose medium, 24 hours of hypoxia caused a massive drop in OCR and complete loss of mitochondrial flexibility in MM iPSC-CMs as non-MM iPSC-CMs maintained responsiveness to oligomycin, FCCP, and antimycin A and rotenone. Twenty-four hours of hypoxia significantly decreased basal respiration, ATP production, and maximal respiration in both non-MM and MM iPSC-CMs where the strongest decrease in OCR was observed in MM iPSC-CMs. Spare respiratory capacity and non-mitochondrial respiration were only significantly decreased in MM iPSC-CMs and not in non-MM iPSC-CMs. Additionally, comparative analysis of non-MM and MM iPSC-CMs cultured in the same plate showed an increased ratio of apoptotic cells ($TUNEL^+$) in MM iPSC-CMs (4 hours, 1% O_2: 23.8% ± 1.5%; 24 hours, 1% O_2: 93.0% ± 2.4% vs 21% O_2: 7.92% ± 1.09%; $P < .001$), while no increase in apoptosis was observed for non-MM iPSC-CMs (4 hours, 1% O_2: 1.18% ± 0.2%; 24 hours, 1% O_2: 10.6% ± 6.6% vs 21% O_2: 1.1% ± 0.23%; $P > .05$; Fig. 4D, 4E). This showed metabolic maturation in MM is responsible for increased sensitivity to hypoxia. Altogether, these results provide further support for our findings that MM iPSC-CMs depend on oxidative phosphorylation and consequently are more sensitive to hypoxia than non-MM iPSC-CMs cultured in glucose-rich or low glucose/lactate media. These results strongly suggest that iPSC-CMs, cultured conventionally and in the presence of glucose, resemble the immature embryonic CM phenotype with respect to their energy substrate utilization, active metabolic pathways, and survival upon low oxygen exposure. In contrast, MM iPSC-CMs cultured with lipids as the primary energy source, more closely resemble adult CMs, consistent with previous reports.[18] We found that MM iPSC-CMs are more sensitive to hypoxia, leading to minimized mitochondrial function, DNA fragmentation, and ultimately apoptosis.

Preconditioning with Nec-1 Protects Metabolically Matured iPSC-CMs from Hypoxic Injury

To determine the utility of our damage model as a platform to screen for protective agents, we preconditioned the cells with the necroptosis inhibitor Nec-1 and assessed whether the previously found protective effects[34,35] could be reproduced (Fig. 5A). Indeed, Nec-1-supplementation 24 hours before induction of hypoxia resulted in significant decrease of cell death compared to non-Nec-1-supplemented controls (fold change EthD1/calcein AM ratio: 0.47 ± 0.06 with Nec-1, $P < .01$; Fig. 5B, 5C). MM iPSC-CMs preconditioned with Nec-1 showed a significant increase in OCR (Fig. 5D, 5E), as opposed to non-MM iPSC-CMs (Supplementary Fig. 3). Furthermore, Nec-1 preconditioning increased the expression of the mitochondrial outer membrane protein TOMM20 compared to control, indicating increased cellular mitochondrial content (Fig. 5F, 5G).

Discussion

In the present study, we confirmed that the conventional method for differentiation of iPSC-CMs using RPMI/B27-based medium (RPMI-Glu/B27) generates cells with low sensitivity to hypoxia and consequential cell death. We furthermore demonstrated that applying metabolic maturation of iPSC-CMs increased sensitivity to hypoxia, rendering these matured cells better models for in vitro models of cardiac ischemia. The observed ability of conventionally cultured, non-MM iPSC-CMs to increase the glycolytic flux in anaerobic conditions is in line with the characteristics of fetal immature CMs having a higher threshold for oxygen insufficiency.[36-38] During development, arterial blood oxygen saturation fluctuates around 3% O_2, which would be considered a hypoxic condition in the adult human heart, with respect to activation of hypoxia-induced gene expression.[37] However, fetal immature CMs are conditioned to low oxygen pressures during development and thus rely on anaerobic energy pathways for metabolism and cardiac growth. Mechanistically, it has been shown that transcription factor hypoxia-inducible factor 1 alpha (HIF1α) is stabilized in fetal CMs under low oxygen pressures and plays a key role in maintaining and enhancing glycolytic metabolism via LDH-A regulation in the compact myocardium and counteracting CM maturation.[23,38,39]

Also in iPSC-CMs the inhibition of HIF1α has been shown to lead to CM maturation and a metabolic shift from aerobic glycolysis toward oxidative phosphorylation.[24] Frequently used "high glucose" cell culture media containing glucose at concentrations of ~15 mmol/L do not relate to human physiology, with local glucose concentrations of ~3 mmol/L, and have been considered obstructive for iPSC-CM maturation.[40] Furthermore, a 4-fold postnatal increase in the concentration of circulating fatty acids enables and drives increased activation of fatty acid β-oxidation pathways in adult CMs.[40,41] Despite relying mainly on the metabolization of glucose, we did observe a decrease in mitochondrial respiration rate in non-MM iPSC-CMs following hypoxia. This could be related to the short intermittent reoxygenation step required for Seahorse metabolic profiling analysis. Cell damage from reperfusion is caused by the release of reactive oxygen species upon the sudden increase in oxygen availability.[42] Hypoxia and reoxygenation have previously been shown to induce only limited damage and prolonged hypoxia without reoxygenation did not affect beating frequency in immature iPSC-CMs.[36] This is in line with our results of maintained beating frequency in immature, non-MM iPSC-CMs after prolonged hypoxia. A previously observed limited effect of hypoxia compared to reperfusion injury on calcium overload-related cellular damage in immature iPSC-CMs,[43] potentially explains why our seahorse results do show a response of iPSC-CMs in RPMI-media to hypoxia. During late human embryonal development, the glycolytic metabolism is insufficient to generate adequate ATP levels for cardiac contractions leading to the metabolic shift toward oxidative phosphorylation.[39] The increased oxygen availability around birth destabilizes the HIF1α transcription factor complex, resulting in the mitochondrial shift toward more energy-efficient oxidative phosphorylation-based metabolism.[38,44] With this increased availability of ATP, CMs mature with a concomitant increase in ploidy, myofibrillar organization, and a number of mitochondria providing for increased energy demands of cardiac contractility.[39] However, these necessary changes in functional and structural phenotypes seem to limit metabolic flexibility. We observed that MM iPSC-CMs, as opposed to non-MM iPS-CMs were sensitive to hypoxia-induced cell death and showed decreased mitochondrial respiration after 4 hours of hypoxia. Additionally, lactate production plays a vital role in glycolysis and was

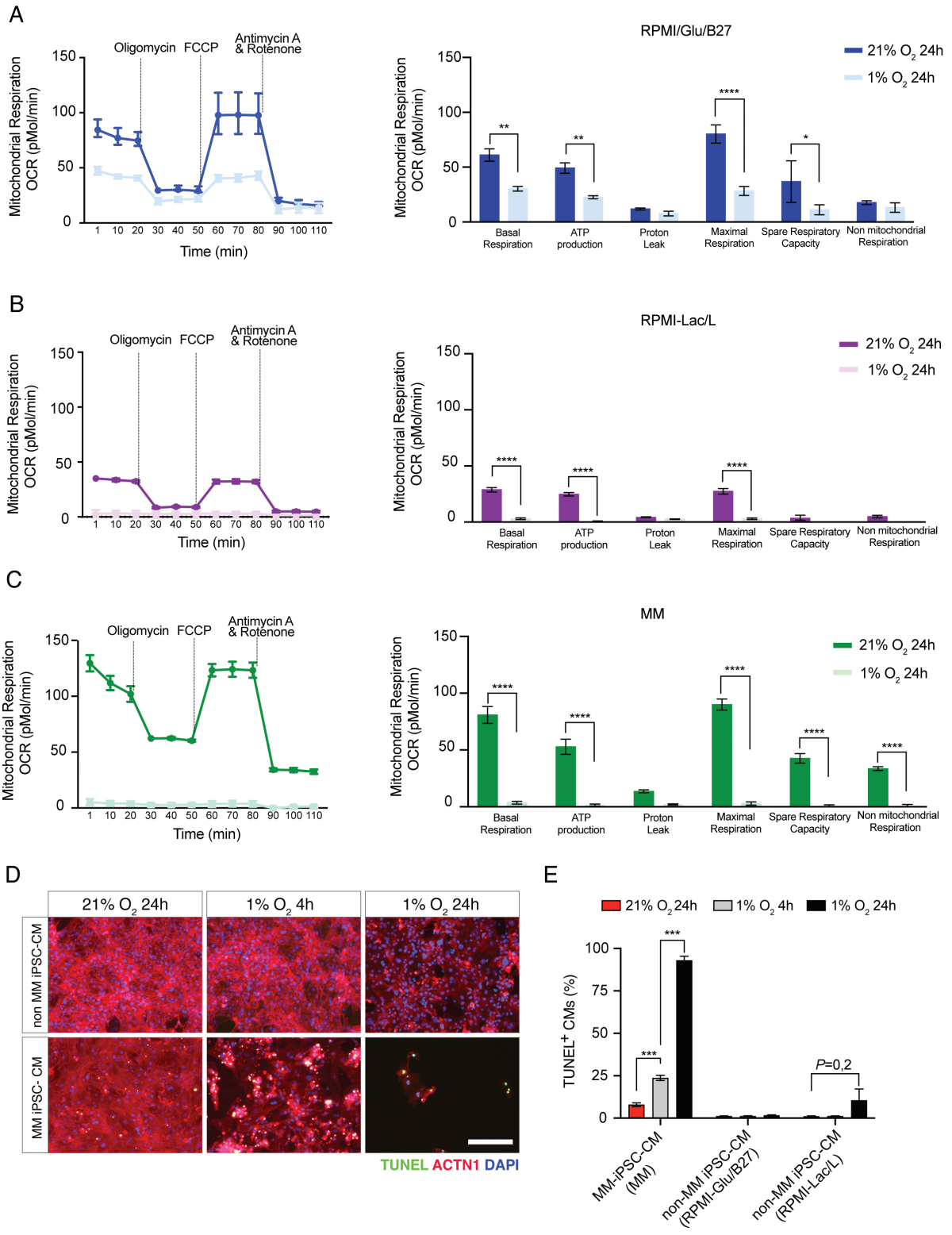

Figure 4. Metabolic profiling of non-MM iPSC-CMs and MM iPSC-CMs exposed to hypoxia. (A-C) Normalized real-time oxygen consumption rate (OCR) of non-MM iPSC-CMs in RPMI-Glu/B27 (A), RPMI-B27 (B), and MM iPSC-CMs (C) in normoxia (21% O_2, 24 hours), short-term hypoxia (1% O_2, 4 hours) or long-term hypoxia (1% O_2, 24 hours) by Seahorse extracellular flux analyzer. Cells were treated with oligomycin, FCCP, and antimycin A and rotenone to measure mitochondrial respiration. (D) Comparative images of TUNEL staining of cardiomyocytes used in metabolic profiling. (E) Quantification of TUNEL staining. A-C: 2 cell lines, 2 biological replicates, 1-2 technical replicates ($n = 5$). Scale bar = 200 µm. Data were analyzed using one-way ANOVA and Dunnett's multiple comparison test. *$P < .05$; **$P < .01$; ***$P < .001$; ****$P < .0001$. Data are shown as mean ± SEM.

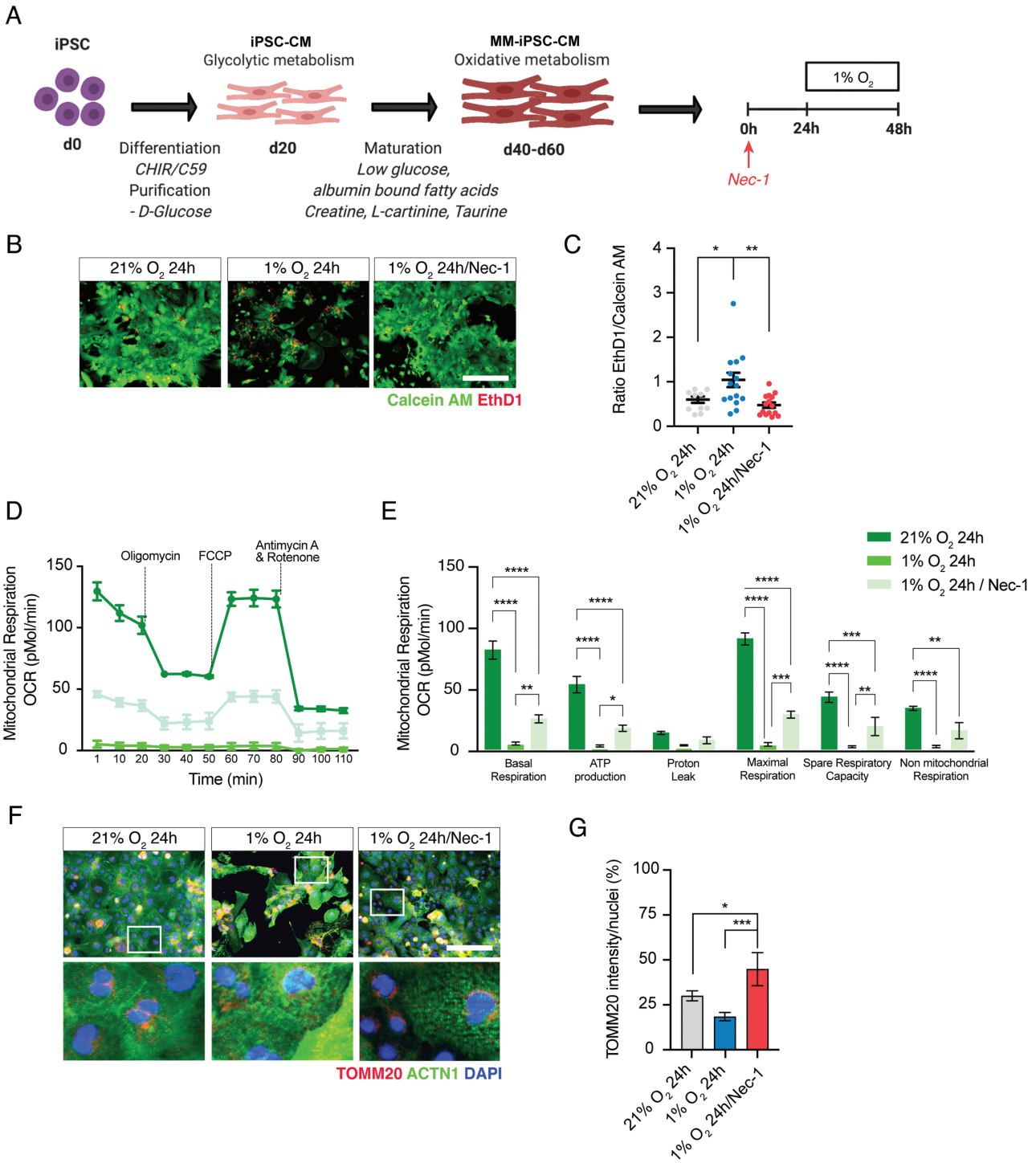

Figure 5. Preconditioning with Nec-1 protects MM iPSC-CMs from hypoxia. (A) Schematic representation of experimental setup. (B) EthD1/calcein AM staining of MM iPSC-CMs exposed to 21% O_2 or 1% O_2 for 24 hours in the absence or presence of necroptosis inhibitor Nec-1. (C) Quantification of B. (D-E) Normalized real-time oxygen consumption rate (OCR) of iPSC-CMs MM iPSC-CMs in normoxia (21% O_2, 24 hours), long-term ischemia (1% O_2, 24 hours), or long-term hypoxia preconditioned with Nec-1 for 24 hours by Seahorse extracellular flux analyzer. Cells were treated with oligomycin, FCCP, and antimycin A and rotenone to measure mitochondrial respiration. (F) Immunofluorescent staining of sarcomeres (ACTN1, green) and mitochondria (TOMM20, red) of cells used for metabolic profiling. (G) Quantification of TOMM20 staining. D-F: 2 cell lines, 2 biological replicates, 1-2 technical replicates ($n = 5$). Scale bar = 200 µm. Data were analyzed using two-way ANOVA. *$P < .05$; **$P < .01$; ***$P < .001$; ****$P < .0001$. Data are shown as mean ± SEM.

not observed in normoxic conditions or in short-term hypoxia, but did increase in long-term hypoxia, indicating that MM iPSC-CMs eventually shift toward oxidative phosphorylation of fatty acids. This observation was in line with the drop in glucose levels in these conditions without an increase in lactate production. Interestingly, we showed that 5% O_2, considered physiological normoxia in most tissue,[33] induced a similar degree of cell death as 1% O_2 for MM iPSC-CMs. This suggests that in our model hypoxia-induced cell death pathways are already induced at a decrease from atmospheric

21% O_2 to 5% O_2, in contrast to previous studies suggesting 0.5%-2% O_2 as effective cellular hypoxia.[43] This difference in physiological tissue normoxia and cell culture normoxia is an important factor to take into account when further developing in vitro hypoxia models. Within this study, differentiation of iPSC to iPSC-CMs is conducted at atmospheric O_2, whereas during cardiac development in vivo CMs differentiate and mature at lower physiological concentrations (5%-8% O_2).[33,37] We have shown that while glycolytic non-MM iPSC-CMs were insensitive to hypoxia, MM iPSC-CMs showed increased sensitivity to hypoxia and even physiological O_2 concentrations. Using a monolayer of a single cell type in an in vitro setting alongside hyperoxia during cardiac differentiation is likely to contribute further to sensitivity to O_2 concentration considered physiological. Further investigation could determine the thresholds of specific O_2 concentrations resulting in activation of hypoxia signaling (eg, HIF1α stabilization) in iPSC-CMs. This could be followed up by hypoxia studies using viable cardiac tissue slices[45] or engineered heart tissues[46] to circumvent limitations of monolayer single cell-type models, although obviously more cost- and technology-intensive, thus probably less promising for high-throughput applications and screens.

Finally, we confirmed the applicability of MM iPSC-CM to model hypoxic damage by validating the protective effects of the necroptosis inhibitor Nec-1, in contrast to conventional, non-MM iPSC-CM culture conditions.

In summary, we have shown that MM iPSC-CMs display increased sensitivity to hypoxic injury, which is more reminiscent of adult CMs and therefore represent an improved model for human ischemic heart disease in vitro.

Acknowledgments

We thank Joseph Wu (Stanford Medicine, USA) for providing the CVI-273 hiPS cell line. We also thank Maike Kreutzenbeck and Rebecca Dieterich (Šarić group, University of Cologne) for their technical support with the generation and characterization of the NP0141-31B/UKKi032-C iPSC line. The authors declare no competing interests.

Funding

M.C.P. and K.N. were supported by the Netherlands Cardiovascular Research Initiative (CVON) [grant No. REMAIN 2014B27] and Health~Holland LSH-TKI [grant No. DELICATE LSHM19086]. M.M. is supported by the National Institutes of Health [grant Nos. 5P01HL141084 and 1R01HL152055] and Foundation Leducq (CUREPLaN). T.Š. was supported by the Innovative Medicine Initiative Joint Undertaking (IMI-JU) funded by the European Commission and the European Federation of Pharmaceutical Industries and Associations (EFPIA, grant agreement No. 115582, "European Bank for induced Pluripotent Stem Cells, EBiSC). J.P.G.S and R.G.C.M were supported by the PLN Foundation. J.P.G.S and A.v.M. were supported by Horizon2020 ERC-2016-COG-EVICARE [grant No. 725229] and BRAVE [grant No. 874827].

Conflict of Interest

The authors declare no potential conflicts of interest.

Author Contributions

M.C.P.: conception and design of experiments, collection and analysis of data, manuscript writing. R.G.C.M.: collection and analysis of data, manuscript writing. I.v.A.: provision of cells. P.M.A.D.: financial support. M.M.: supervision project, administrative support. T.Š.: provision of cells. J.W.B.: supervision project. A.v.M.: provision of cells. S.A.J.C.: conception and design experiments, financial support, supervision project. J.P.G.S.: conception and design experiments, supervision project. A.P.H.: supervision project. K.N.: conception and design experiments, supervision project, manuscript writing, financial support

Data Availability

The data that support the findings of this study are available from the corresponding author upon reasonable request.

Supplementary Material

Supplementary material is available at *Stem Cells Translational Medicine* online.

References

1. Virani SS, Alonso A, Benjamin EJ, et al. Heart disease and stroke statistics—2020 update: a report from the American Heart Association. *Circulation*. 2020;141(9):e139-e596. https://doi.org/10.1161/CIR.0000000000000757
2. Oerlemans MIFJ, Koudstaal S, Chamuleau SA, et al. Targeting cell death in the reperfused heart: pharmacological approaches for cardioprotection. *Int J Cardiol*. 2013;165(3):410-422. https://doi.org/10.1016/j.ijcard.2012.03.055
3. Hausenloy DJ, Garcia-Dorado D, Bøtker HE, et al. Novel targets and future strategies for acute cardioprotection: position paper of the European Society of Cardiology Working Group on Cellular Biology of the Heart. *Cardiovasc Res*. 2017;113(6):564-585. https://doi.org/10.1093/cvr/cvx049
4. Ferdinandy P, Hausenloy DJ, Heusch G, Baxter GF, Schulz R. Interaction of risk factors, comorbidities, and comedications with ischemia/reperfusion injury and cardioprotection by preconditioning, postconditioning, and remote conditioning. *Pharmacol Rev*. 2014;66(4):1142-1174. https://doi.org/10.1124/pr.113.008300
5. Milani-Nejad N, Janssen PML. Small and large animal models in cardiac contraction research: advantages and disadvantages. *Pharmacol Ther*. 2014;141(3):1-5. https://doi.org/10.1016/j.pharmthera.2013.10.007
6. Pond AL, Scheve BK, Benedict AT, et al. Expression of distinct ERG proteins in rat, mouse, and human heart. Relation to functional I(Kr) channels. *J Biol Chem*. 2000;275(8):5997-6006. https://doi.org/10.1074/jbc.275.8.5997
7. Swynghedauw B. Developmental and functional adaptation of contractile proteins in cardiac and skeletal muscles. *Physiol Rev*. 1986;66(3):710-771. https://doi.org/10.1152/physrev.1986.66.3.710
8. Marian AJ. On mice, rabbits and human heart failure. *Circulation*. 2005;111(18):2276-2279. https://doi.org/10.1161/01.CIR.0000167559.13502.9A
9. Uosaki H, Taguchi YH. Comparative gene expression analysis of mouse and human cardiac maturation. *Genomics Proteomics Bioinformatics*. 2016;14(4):207-215. https://doi.org/10.1016/j.gpb.2016.04.004
10. Karakikes I, Ameen M, Termglinchan V, Wu JC. Human induced pluripotent stem cell-derived cardiomyocytes: insights into molecular, cellular, and functional phenotypes. *Circ Res*. 2015;117(1):80-88. https://doi.org/10.1161/CIRCRESAHA.117.305365
11. Takahashi K, Tanabe K, Ohnuki M, et al. Induction of pluripotent stem cells from adult human fibroblasts by defined factors. *Cell*. 2007;131(5):861-872. https://doi.org/10.1016/j.cell.2007.11.019

12. Burridge PW, Keller G, Gold JD, Wu JC. Production of de novo cardiomyocytes: human pluripotent stem cell differentiation and direct reprogramming. *Cell Stem Cell*. 2012;10(1):16-28. https://doi.org/10.1016/j.stem.2011.12.013
13. van Mil A, Balk GM, Neef K, et al. Modelling inherited cardiac disease using human induced pluripotent stem cell-derived cardiomyocytes: progress, pitfalls, and potential. *Cardiovasc Res*. 2018;114(14):1828-1842. https://doi.org/10.1093/cvr/cvy208
14. Li Q, Wang J, Wu Q, Cao N, Yang HT. Perspective on human pluripotent stem cell-derived cardiomyocytes in heart disease modeling and repair. *Stem Cells Transl Med*. 2020;9(10):1121-1128. https://doi.org/10.1002/sctm.19-0340
15. Hnatiuk AP, Briganti F, Staudt DW, Mercola M. Human iPSC modeling of heart disease for drug development. *Cell Chem Biol* 2021;28(3):271-282. https://doi.org/10.1016/j.chembiol.2021.02.016
16. Robertson C, Tran DD, George SC. Concise review: maturation phases of human pluripotent stem cell-derived cardiomyocytes. *Stem Cells*. 2013;31(5):829-837. https://doi.org/10.1002/stem.1331
17. Herron TJ. Calcium and voltage mapping in hiPSC-CM monolayers. *Cell Calcium*. 2016;59(2-3):84-90. https://doi.org/10.1016/j.ceca.2016.02.004
18. Feyen DAM, McKeithan WL, Bruyneel AAN, et al. Metabolic maturation media improve physiological function of human iPSC-derived cardiomyocytes. *Cell Rep*. 2020;32(3):107925. https://doi.org/10.1016/j.celrep.2020.107925
19. Ulmer BM, Eschenhagen T. Human pluripotent stem cell-derived cardiomyocytes for studying energy metabolism. *Biochim Biophys Acta Mol Cell Res*. 2020;1867(3):118471. https://doi.org/10.1016/j.bbamcr.2019.04.001
20. Tohyama S, Hattori F, Sano M, et al. Distinct metabolic flow enables large-scale purification of mouse and human pluripotent stem cell-derived cardiomyocytes. *Cell Stem Cell*. 2013;12(1):127-137. https://doi.org/10.1016/j.stem.2012.09.013
21. Fillmore N, Levasseur JL, Fukushima A, et al. Uncoupling of glycolysis from glucose oxidation accompanies the development of heart failure with preserved ejection fraction. *Mol Med*. 2018;24(1):3. https://doi.org/10.1186/s10020-018-0005-x
22. Ulmer BM, Stoehr A, Schulze ML, et al. Contractile work contributes to maturation of energy metabolism in hiPSC-derived cardiomyocytes. *Stem Cell Reports*. 2018;10(3):834-847. https://doi.org/10.1016/j.stemcr.2018.01.039
23. Horikoshi Y, Yan Y, Terashvili M, et al. Fatty acid-treated induced pluripotent stem cell-derived human cardiomyocytes exhibit adult cardiomyocyte-like energy metabolism phenotypes. *Cells*. 2019;8(9):1095. https://doi.org/10.3390/cells8091095
24. Hu D, Linders A, Yamak A, et al. Metabolic maturation of human pluripotent stem cell derived cardiomyocytes by inhibition of HIF1α and LDHA. *Circ Res*. 2018;123(9):1066-1079. https://doi.org/10.1161/CIRCRESAHA.118.313249
25. Hidalgo A, Glass N, Ovchinnikov D, et al. Modelling ischemia-reperfusion injury (IRI) in vitro using metabolically matured induced pluripotent stem cell-derived cardiomyocytes. *APL Bioeng*. 2018;2(2):026102. https://doi.org/10.1063/1.5000746
26. Kitani T, Ong SG, Lam CK, et al. Human-induced pluripotent stem cell model of trastuzumab-induced cardiac dysfunction in patients with breast cancer. *Circulation*. 2019;139(21):2451-2465. https://doi.org/10.1161/CIRCULATIONAHA.118.037357
27. Matsa E, Burridge PW, Yu KH, et al. Transcriptome profiling of patient-specific human iPSC-cardiomyocytes predicts individual drug safety and efficacy responses in vitro. *Cell Stem Cell*. 2016;19(3):311-325. https://doi.org/10.1016/j.stem.2016.07.006
28. Hamad S, Derichsweiler D, Papadopoulos S, et al. Generation of human induced pluripotent stem cell-derived cardiomyocytes in 2D monolayer and scalable 3D suspension bioreactor cultures with reduced batch-to-batch variations. *Theranostics*. 2019;9(24):7222-7238. https://doi.org/10.7150/thno.32058
29. Schneider CA, Rasband WS, Eliceiri KW. NIH Image to ImageJ: 25 years of image analysis. *Nat Methods*. 2012;9(7):671-675. https://doi.org/10.1038/nmeth.2089
30. Ye L, Qiu L, Zhang H, et al. Cardiomyocytes in young infants with congenital heart disease: a three-month window of proliferation. *Sci Rep*. 2016;6:1-9. https://doi.org/10.1038/srep23188
31. Kretzschmar K, Post Y, Bannier-Hélaouët M, et al. Profiling proliferative cells and their progeny in damaged murine hearts. *Proc Natl Acad Sci USA*. 2018;115(52):E12245-E12254. https://doi.org/10.1073/pnas.1805829115
32. Balafkan N, Mostafavi S, Schubert M, et al. A method for differentiating human induced pluripotent stem cells toward functional cardiomyocytes in 96-well microplates. *Sci Rep*. 2020;10(1):1-14. https://doi.org/10.1038/s41598-020-73656-2
33. Carreau A, El Hafny-Rahbi B, Matejuk A, Grillon C, Kieda C. Why is the partial oxygen pressure of human tissues a crucial parameter? Small molecules and hypoxia. *J Cell Mol Med*. 2011;15(6):1239-1253. https://doi.org/10.1111/j.1582-4934.2011.01258.x
34. Oerlemans MIFJ, Liu J, Arslan F. Inhibition of RIP1-dependent necrosis prevents adverse cardiac remodeling after myocardial ischemia-reperfusion in vivo. *Basic Res Cardiol*. 2012;107(4):270. https://doi.org/10.1007/s00395-012-0270-8
35. Feyen D, Gaetani R, Liu J, et al. Increasing short-term cardiomyocyte progenitor cell (CMPC) survival by necrostatin-1 did not further preserve cardiac function. *Cardiovasc Res*. 2013;99(1):83-91. https://doi.org/10.1093/cvr/cvt078
36. Häkli M, Kreutzer J, Mäki AJ, et al. Human induced pluripotent stem cell-based platform for modeling cardiac ischemia. *Sci Rep*. 2021;11(1):1-13. https://doi.org/10.1038/s41598-021-83740-w
37. Patterson A J, Zhang L. Hypoxia and fetal heart development. *Curr Mol Med*. 2010;10(7):653-666. https://doi.org/10.2174/156652410792630643
38. Ascuitto RJ, Ross-Ascuitto NT. Substrate metabolism in the developing heart. *Semin Perinatol*. 1996;20(6):542-563. https://doi.org/10.1016/s0146-0005(96)80068-1
39. Menendez-Montes I, Escobar B, Palacios B, et al. Myocardial VHL-HIF signaling controls an embryonic metabolic switch essential for cardiac maturation. *Dev Cell*. 2016;39(6):724-739. https://doi.org/10.1016/j.devcel.2016.11.012
40. Slaats RH, Schwach V, Passier R. Metabolic environment in vivo as a blueprint for differentiation and maturation of human stem cell-derived cardiomyocytes. *Biochim Biophys Acta Mol Basis Dis*. 2020;1866(10):165881.https://doi.org/10.1016/j.bbadis.2020.165881
41. Lopaschuk GD, Jaswal JS. Energy metabolic phenotype of the cardiomyocyte during development, differentiation, and postnatal maturation. *J Cardiovasc Pharmacol*. 2010;56(2):130-140. https://doi.org/10.1097/FJC.0b013e3181e74a14
42. Ferrari R, Ceconi C, Curello S, et al. Role of oxygen free radicals in ischemic and reperfused myocardium. *Am J Clin Nutr*. 1991;53(1 Suppl):215S-222S. https://doi.org/10.1093/ajcn/53.1.215S
43. Wei W, Liu Y, Zhang Q, et al. Danshen-enhanced cardioprotective effect of cardioplegia on ischemia reperfusion injury in a human-induced pluripotent stem cell-derived cardiomyocytes model. *Artif Organs*. 2017;41(5):452-460. https://doi.org/10.1111/aor.12801
44. Neary MT, Ng KE, Ludtmann MHR, et al. Hypoxia signaling controls postnatal changes in cardiac mitochondrial morphology and function. *J Mol Cell Cardiol*. 2014;74:340-352. https://doi.org/10.1016/j.yjmcc.2014.06.013
45. Pitoulis FG, Watson SA, Perbellini F, Terracciano CM. Myocardial slices come to age: an intermediate complexity in vitro cardiac model for translational research. *Cardiovasc Res*. 2020;116(7):1275-1287. https://doi.org/10.1093/cvr/cvz341
46. Giacomelli E, Meraviglia V, Campostrini G, et al. Human-iPSC-derived cardiac stromal cells enhance maturation in 3D cardiac microtissues and reveal non-cardiomyocyte contributions to heart disease. *Cell Stem Cell*. 2020;26(6):862-879.e11. https://doi.org/10.1016/j.stem.2020.05.004